Spring 1-1-2013

A Buoyancy-Decoupling Approach to Cookstove Modeling and Quantification Methods for Metal Oxide Type Pollutant Sensors

Nicholas Bantle Masson
University of Colorado Boulder, nicholas.b.masson@gmail.com

A Buoyancy-Decoupling Approach to Cookstove Modeling and Quantification Methods for Metal Oxide Type Pollutant Sensors

by

N. B. Masson

A thesis submitted to the

Faculty of the Graduate School of the

University of Colorado in partial fulfillment

of the requirements for the degree of

Masters of Science

Department of Mechanical Engineering

2013

This thesis entitled:
A Buoyancy-Decoupling Approach to Cookstove Modeling and Quantification Methods for Metal Oxide Type Pollutant Sensors
written by N. B. Masson
has been approved for the Department of Mechanical Engineering

_____
Michael Hannigan

_____
Prof. Shelly Miller

_____
Prof. Peter Hamlington

Date _____

The final copy of this thesis has been examined by the signatories, and we find that both the content and the form meet acceptable presentation standards of scholarly work in the above mentioned discipline.

Masson, N. B. (M.S., Mechanical Engineering)

A Buoyancy-Decoupling Approach to Cookstove Modeling and Quantification Methods for Metal Oxide Type Pollutant Sensors

Thesis directed by Prof. Michael Hannigan

Nearly half the world's population cooks with wood and charcoal, most of which is used in open "three stone fires" or inefficient cookstoves. These methods are so "dirty" that they produce one quarter of global carbon dioxide emissions and result in levels of respiratory illness rivaling the worldwide disease burden of HIV/AIDS. A clean cookstove, designed to make the combustion process less polluting and more thermally efficient, could significantly mitigate the detrimental health and environmental effects of biomass burning.

This work has two foci. The first is to develop a method for better stove modeling and design. In particular, an empirical correlation is developed between combustion rate and bulk fluid flow in a forced convection stove case. This is coupled with computational models of stove operation in which fluid flow is a function of a constant heat flux. A parameter study between both cases gives sufficient data to determine where one would expect operating conditions to stabilize in a natural draft (buoyancy driven) cookstove.

The second part of this work focuses on developing a quantification model for metal oxide type semiconductor sensors. These sensors are common in low-cost pollutant sensing applications, but their response has yet to be quantified with the accuracy necessary for the ambient monitoring of pollution.

Together, these two sections provide tools for the design as well as the validation of cookstoves. Both steps are necessary if cookstoves are to be confidently disseminated as a significant and beneficial technology.

Acknowledgements

Thank you to BURN Design Lab on Vashon Island, Washington, for the support and help in collecting experimental data during the Summer of 2012.

Most of all, thank you to Professor Michael Hannigan for the continued support and encouragement in my academic pursuits.

Contents

Chapter

Tables

Table

Figures

Figure

Chapter 1

Introduction

There are two types of stoves: clean stoves and dirty stoves. Clean stoves accomplish the task of cooking and household heating with minimal pollutant emissions. Dirty stoves accomplish the same task at the expense of significant indoor air pollution and detriment to personal health. Most stoves are dirty stoves.

For half the world's population, cooking means being exposed to the harmful effects of burning coal and biomass. The inefficient combustion of biomass accounts for high indoor concentrations of particulate matter (PM) – two indoor air pollutants which pose significant health risks. The World Health Organization (WHO) estimates that exposure to smoke may be responsible for "nearly 2 million excess deaths in the developing countries, and for some 4% of the global burden of disease"[10]. This is equivalent to the number of deaths due to HIV/AIDS. In many cultures this burden of disease disproportionately affects women and young children who spend much of their time cooking indoors[31]. Furthermore, the use of biomass as a primary fuel in the developing world results in an estimated 25% of global carbon dioxide (CO_2) emissions, and is a leading cause of deforestation. In Kenya, for example, wood gathering has contributed to the destruction of 94% of the original native forest, placing pressure on both the ecosystem and local communities.

Consider two solutions. Stop cooking or make cooking a clean process. The first is not plausible. Cooking is not only cultural, but, as Harvard anthropologist Richard Wragham argues, has influenced the very nature of our evolution[22]. We are designed to eat cooked food[23]. How, then, can cooking be made clean?

In many of these regions, biomass is burned in an open "three stone fire", resulting in significant sooting and pollution as well as inefficient use of energy. The introduction of cookstove technology can dramatically reduce all of these adverse effects. The widespread dissemination of cookstoves, however, cannot adhere to the paradigm of "one size fits all".

The broad scope of this work involves extending the state of the art with respect to both cookstove design and emissions/exposure assessment. Both pieces are critical in instigating meaningful global change.

The first part of this work concerns the development of a specific methodology for improving the stove modeling and design process. Specifically, the fluid flow and heat release process is empirically decoupled and used to improve the current methods in computational modeling of cookstove design.

The second part of this work addresses the quantification of gas-phase pollutant emissions from cookstoves. This can be in the form of direct emissions from the cookstove or personal exposure of those in the cookstove vicinity. In particular, a quantification method is developed for one type of inexpensive pollutant sensor. With proper quantification schemes, these sensors can be implemented in many types of pollutant monitoring applications.

1.0.1 Stove Design

Cookstoves must be designed on a regional or state-wide basis, taking into account cooking practices, fuel type, user habits, etc... To date, the design of "clean cookstoves" has relied predominantly on experimental data[9][27] and general principles of combustion and heat transfer to maximize stove performance[6]. The iterative design process involves a prototype/test/redesign cycle until a stove meets acceptable standards.

Basic design rules exist for the design of common stove types, such as the popular 'Rocket Stove'. Constraining aspect ratios and material choice, for example, help to produce a fuel efficient and less polluting cookstove. Maximizing performance, however, often requires incorporating complex geometries, which affect heat transfer and fluid flow in ways that require analysis beyond that

found in basic design guidelines.

1.0.2 Stove Modeling

The use of computational and numerical modeling can complement the design process by optimizing a specific stove's design and pushing overall performance standards beyond those achieved with basic design rules. Running a model is often less time and resource intensive than iterating through a test/redesign cycle.

Modeling efforts have focused on both better quantifying the combustion process and the fluid dynamics/heat transfer which describe cookstove performance[1][29][12] . While computational modeling proves to be a valuable tool, it has nonetheless failed to influence the design process for the many companies manufacturing cookstoves. In general, the design and development of cookstoves is carried out by small firms who cannot hire a full time modeler. This often prevents the implementation of complex models, which require extensive knowledge of running computational simulations and modeling software.

The approach here presented focuses on the usability of simulation tools rather than pushing the fidelity of computational models. Modeling is seen as a complement to the iterative design process rather than a replacement. In particular, this work focuses on using empirical measurements in conjunction with computational fluid dynamics to better approximate the heat release due to combustion. Runtime, usability and complexity ar greatly improved by approximating the complex combustion dynamics.

1.0.3 Stove Validation

A stove's performance can be evaluated under two distinct criteria: health and environment. Health performance refers to a stove's ability to reduce the production of harmful pollutants. Functionally this is related to the quality of the combustion process. Environmental performance refers to a stove's thermodynamic efficiency and ability to maximize heat transfer to the cooking receptacle. This ultimately reduces the production of carbon dioxide entering the atmosphere and

minimizes fuel use, thus mitigating the rate of deforestation.

The most common test for a stove's thermodynamic efficiency is the "water boiling test" (WBT) [36][5] . The WBT is meant as a tool to be used in a controlled environment to assess a stove's performance under several common operating scenarios. These include *a*) a cold-start, where the stove is used at maximum power (fastest burn-rate achievable) starting at room temperature; *b*) a hot-start, which is the same as the cold-start accept begins with a pre-heated stove; and *c*) a simmer test, where the stove is turned-down to keep water just below boiling for 45 minutes. The WBT uses a standard volume of water and pot size. The time to boil gives a measure of net heat transfer to the pot for tests *a)* and *b)*. The fuel is weighed before and after each test to determine net fuel consumption. The WBT gives useful metrics such as a stove's time to boil, burn rate, heating rate, fuel consumption, turn-down ratio (ratio of high power to simmer power) and net thermal efficiency.

The WBT gives good standard data with which to inter-compare stove models. It does not, however, account for variability encountered when cooking real meals. A variant of the WBT, the Controlled Cooking Test (CCT)[4] is caried out in the field as is a means to test the 'real life' performance of a cookstove under specific user conditions.

The health or emissions performance is not widely measured as it requires more complex instrumentation than that used for the WBT or CCT. An emission measuring system typically consists of an enclosure for capturing a stove's exhaust, and an assortment of sensors to measure CO, CO_2 and PM. It is often desirable to also segregate particulate matter size, and only measure fine and ultra-fine PM below 2.5 microns in size ($PM_{2.5}$). The PM produced by cookstoves in the form of smoke, however, can typically be assumed to be entirely ultrafine.

Systems for cookstove emissions measurements do exist, such as Aprovecho's Portable Emissions Measurement System (PEMS) yet they remain largely unused amongst the stove development community. Such systems tend to be costly and are not widely available.

The growing field of low-cost air quality sensors shows great promise when applied to cookstove development and performance assessment. This includes both direct measurement of cook-

stove emissions as well as personal exposure to ambient pollutants. This work addresses the quantification and implementation of low-cost sensing technology, with an emphasis on usability in personal exposure assessment.

1.0.4 Health and Personal Exposure Assessment

Personal exposure to harmful pollutants is intricately linked with the performance and emissions of cookstoves. Understanding the health risks and quantifying exposure, however, extends beyond the cookstove to include factors such as user habit, kitchen/cook-area ventilation, meal type and stove use, etc... Measuring direct stove emissions in conjunction with personal exposure provides sufficient data to capture the entire system and the many parameters affecting exposure variability.

Wearable exposure monitors are a useful means for monitoring real-time exposure to combustion pollutants. These monitors can be in the form of small particulate matter filter samplers or one of several devices in the bourgeoning field of low-cost environmental sampling. The UPOD[28] developed at the University of Colorado at Boulder is one such device.

Low-cost sensing technology enables widespread sampling of pollutants which is otherwise unattainable with current instruments. Many challenges exist, however, in quantifying the signal response from inexpensive sensors. Most sensor signals require extensive post-processing to account for interference affects and non-linear response characteristics.

The final section of this work addresses methodology for quantifying the signal response from metal oxide type (MOx) sensors. The quantification model and calibration scheme are specifically derived given the preface of usability and practicality. Using the proposed model and calibration method makes MOx technology one attractive pollutant sensing technology in context of personal exposure and remote sensing applications.

Chapter 2

Principles of Stove Operation

2.0.5 The Basics

A stove is nothing more than an enclosure in which a combustion process is used to create concentrated heat. The major engineering components can be broken down into three principles: combustion, fluid flow and heat transfer. The combustion is typically achieved by burning wood, charcoal or other biomass. The fluid flow is driven by the buoyant updraft of hot air, which both serves to advect heat towards the pot (or other receptacle), as well as entrain fresh air needed for the combustion process. When a stove is used exclusively for cooking, then it is advantageous to maximize heat transfer to the stove surface and minimize heat transfer to the surrounding environment.

A stove has one main advantage over an open three stove fire: concentration. By enclosing the combustion area, a stove maximizes heat retention within the combustion region. This has the beneficial affects of maximizing temperature, turbulence and entrained oxygen, all of which improve combustion efficiency and completeness.

Many traditional wood burning stoves have been designed using ten principles [11] devised to maximize combustion efficiency and heat transfer. These include guidelines such as insulating the stove with light-weight material of low thermal mass or using a combustion chamber with a height approximately three times that of its diameter. Tabulated data exists which gives suggested stove aspect ratios based on experimental observation.

Maximizing stove efficiency, however, requires going beyond basic design rules. This often

includes incorporating more complex design feature such as secondary air injection via cowlings. The effectiveness of such features is difficult to assess without more complex analysis. A stove in operation will be also be significantly affected by fuel type and variability, pot size, cook-time, user habits etc... These parameters must be considered when designing a cookstove.

2.0.6 Coupled System

The governing principles that drive the combustion and heat transfer process in cookstoves are highly coupled and incredibly complex. Variability in the input parameters (eg. fuel type/ position/ geometry/ quantity) make optimization of stove performance a notable challenge.

As mentioned in the previous section, the driving mechanisms of stove operation include combustion, fluid flow and heat transfer. These mechanisms are not only complex in and of themselves, but are interdependent. Anyone who has built a fire knows this intuitively. Blowing on a fire (increase fluid flow) tends to increase the rate of combustion by making more oxygen available to the combustion process. Too much flow, however, and one risks extinguishing the flame by stretching the flame combustion region to the extent where the fuel-air decreases sufficiently in temperature as to quench the combustion process.

In a wood-fired stove, the natural buoyant draft provides this 'blowing' fluid flow. The strength of this flow depends on the air temperature (influenced by the combustion and heated stove walls), hence the heat transfer. The list of interconnected cause-effect relationships goes on.

2.2 gives a very simplistic diagram of some significant relationships driving natural convection combustion processes. In particular, note the coupling of the fluid flow with the fluid temperature (due to combustion heat release).

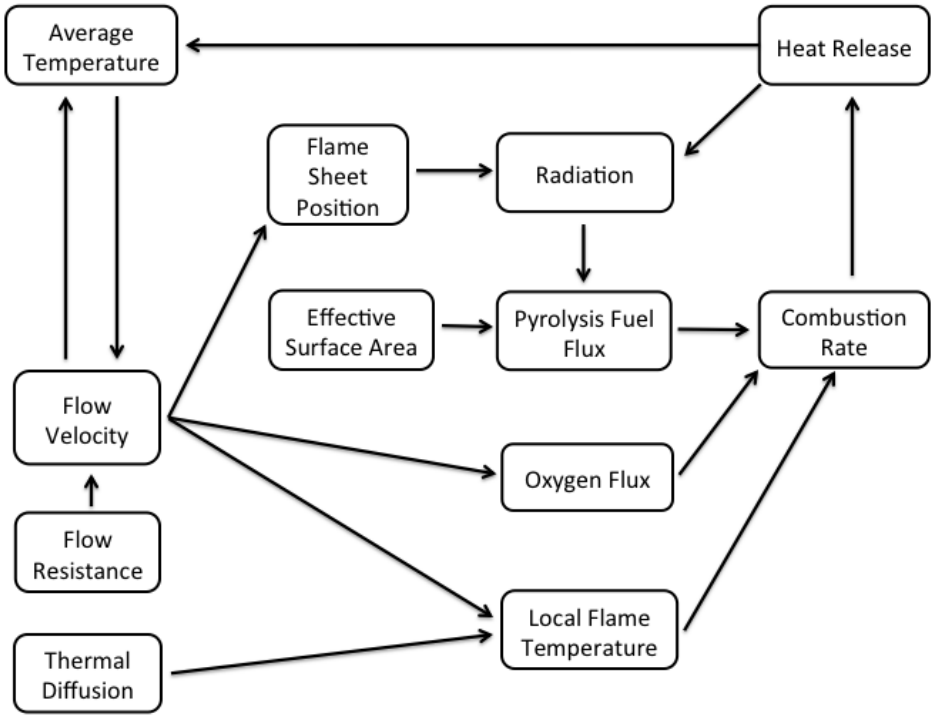

Figure 2.1: Diagram for Stove Operation Parameters

This feedback mechanism is that which drives the combustion process in the above wood-stove example. Where the stove finds its natural operating state depends on this feedback coupling between buoyant temperature driven flow and combustion rate.

2.0.7 Pyrolysis and Combustion

The combustion process is arguably the most complex component of a stove's operation. The combustion of solid biomass can be separated into two distinct types: a homogeneous phase reaction with the products of pyrolysis and a heterogeneous phase reaction with solid char.

When woody biomass fuel is exposed to high temperature and low oxygen environments, it will thermally decompose into volatile gases, tar and char. This is known as pyrolysis. Gasification (volatilization with minimal oxidation), typically occurs at fuel-air equivalence ratios (ϕ) of $\phi = 0.25 - 3$. The equivalence ratio is defined as quotient of the fuel-to-oxidizer ratio relative to the

stoichiometric fuel-to-oxidizer ratio. Under most operating conditions, wood combustion results in an adiabatic flame temperature (AFT) of approximately 2050°C, though this varies depending on the gas mixture produced by pyrolysis. The constituents of the volatile gases and tar vary depending on the material and the conditions under which it is pyrolyzed. High temperature conditions, for example, tend to result in rapid pyrolysis with more volatiles and less char formation. The pyrolysis front will propagate through the material, providing a consistent flux of volatile, combustible gases from the solid fuel's surface. The gases entrain and react with air from the ambient environment. The reaction typically creates a thin flame sheet as the reaction time is far faster than that of the advecting reactants. The radiative forcing from the flame sheet perpetuates the cycle of pyrolysis and combustion.

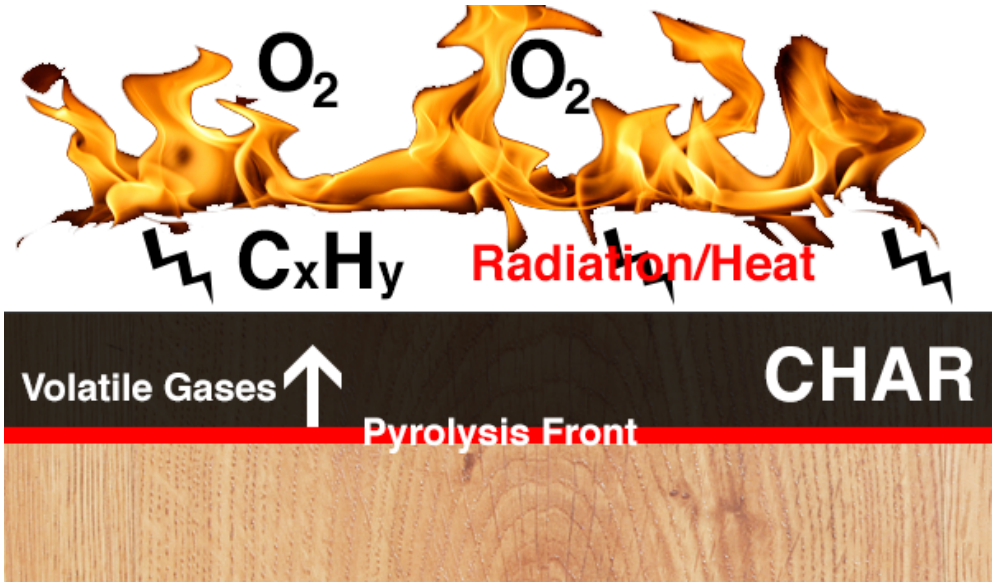

Figure 2.2: Diagram for Stove Operation Parameters

The solid char, which is predominantly carbon, undergoes a heterogeneous phase reaction in which the solid carbon is oxidized by gas phase reactants. During the initial stages of combustion, the flux of pyrolysis products from the solid fuel surface prevents ambient oxygen from diffusing through the flame front and reacting with the char. Some of the pyrolysis products do react with

the char itself, but this is negligible relative to the combustion process of the volatile pyrolysis gases. As such, the heterogeneous char reaction is secondary to that of pyrolysis during the initial stages of combustion. During later stages of combustion, the volatile matter becomes exhausted and the process is dominated by heterogeneous reactions of ambient oxygen and char.

Charcoal stoves differ in that charcoal is woody biomass, which has already been pyrolyzed, leaving only the carbon char as fuel. The combustion observed in charcoal stoves is then far simpler as it only consists of the heterogeneous reaction of oxygen and the solid carbon fuel.

Quantifying the combustion process is exceedingly difficult for most practice applications. A comprehensive model would need to include the transient propagation of the pyrolysis front in all directions – both propagation normal to the fuel surface and spread tangent to the fuel surface [16] (i.e. solid fuel is never evenly lit and evenly burning). Pyrolysis is also be affected by wood grain orientation, fuel type and moisture content [2]. Incident heating rates must be known in addition to material properties such as char porosity (which affects pyrolysis product diffusion rates) and char thermal characteristics (which affect the heat conduction through the material to the pyrolysis front).

Models must also include the gas-phase combustion process, which drives both pyrolysis and fluid flow within the stove. This requires knowing the products of pyrolysis, their transport characteristics and the reaction mechanisms. Understanding complex combustion also requires modeling complex fluid dynamics, as the turbulent transport of reactants into the combustion region is crucial to the process.

2.0.8 Combustion Modeling

Much work has been carried out to characterize the fundamental processes and products of pyrolysis[14][15]. This includes both theoretical models of the pyrolysis process[21][20][13][35] and experimentally measuring the products of pyrolysis[34][30].

Several experimental methods are used in assessing both the products and heat of combustion (ΔH_c°). The methods differ in how heat is applied to the sample biomass. Thermogravimetic

analysis (TGA) consists of heating a sample at either constant temperature (isothermal TGA) or at constant heating rate (dynamic TGA). Differential thermal analysis (DTA) and differential scanning calorimetry (DSC) are similar methods in which the heating rate of a sample is measured relative to a reference. Sample and reference are held at the same temperature (either constant temperature or identical temperature profiles). The difference in heating rate provides information as to the endothermic or exothermic nature of the reaction. Pyrolysis has been seen to be both endothermic and exothermic under different conditions. This indicates the significant variability in the many elementary processes which contribute to pyrolysis).

2.0.9 Closure from Empirical Observations

It should now be evident that the processes contributing to combustion are incredibly complex and difficult to model. The computational might and model complexity often preclude the useful application of extensive combustion modeling in cookstove design.

2.3 is a simplification of 2.2 where the intricacies of combustion have been replaced by an empirically derived relationship between the bulk fluid flow rate and the heat of combustion.

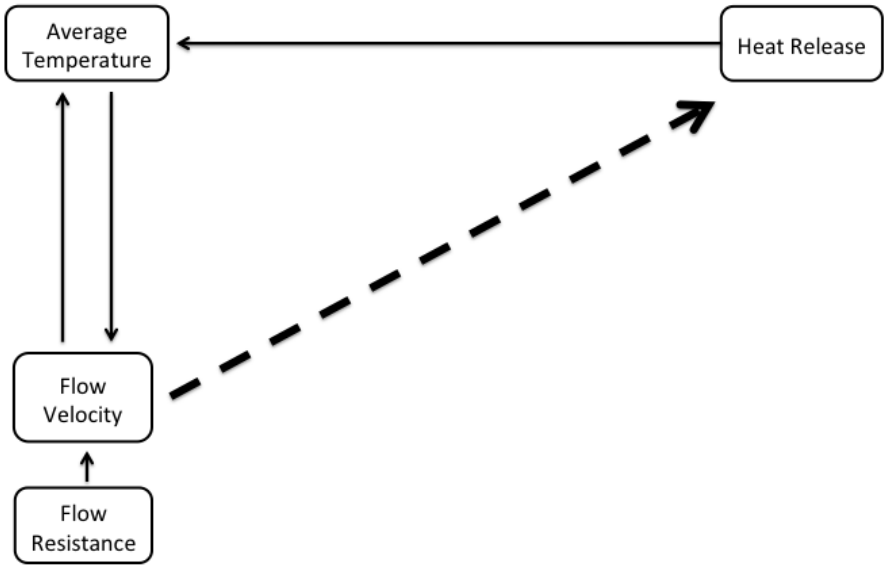

Figure 2.3: Feedback Diagram with Empirical Closure

First consider the effect of heat release on fluid flow. Simple buoyant flow models or more complex CFD models can be used to assess the expected fluid flow for a fixed heat release rate and a given stove geometry. It is common in stove modeling to assume a fixed heat release rate from the fuel surface, and to take fluid flow to be the dependent parameter.

These models, however, do not take into account how the fluid flow rate affects the heat release from the burning fuel. An empirically derived relationship taking heat release as the dependent parameter can inform CFD models as to whether or not the value of a constant heat release can be reasonably expected given the resulting fluid flow.

The relationship between heat release and fluid flow can be examined by using forced convection (controlled flow), effectively decoupling the buoyant mechanism driving flow in natural convection. Iterating through different flow velocities and measuring heat release gives the empirical relationship.

It should be noted that this relationship also depends on the fuel sample size, geometry,

orientation, type, specific area, moisture content, etc... The goal of this work is to validate the above-mentioned method of empirically decoupling the buoyant flow combustion process. As such, experiments were carried out for only one specific wood type, geometry etc... In practice, flow/heat-release relationships would need to be determined for each of the above factor combinations. Then a stove designer might lookup the relationship for the specific fuel conditions considered in the stove design.

Chapter 3

Experimental Instrumentation

3.0.10 Experimental Setup

The experimental instrumentation was constructed using readily available material and low-cost measurement devices. The system consisted of 3 main components: a stove prototype, a forced convection system for controlling bulk fluid flow (decoupling buoyancy from the driving forces) and an emissions measurement system for assessing combustion rate.

A simplistic stove prototype was constructed by rolling and spot-welding steel sheet metal into a 6-inch diameter cylinder. The bottom of the cylinder reduced to a short 3-inch diameter section. A steel grate for holding fuel was placed at approximately 8 inches from the cylinder top.

The forced air convection system was built using 3 inch diameter PVC pipe with a right angle coupling to connect to the stove prototype. The far end of the PVC pipe housed a small DC fan attached to a laser cut mounting plate. An inexpensive hot wire anemometer from Modern Devices was glued into the centerline of the PVC pipe.

A UPOD[28] data acquisition and microcontroller system was customized to provide feedback between the anemometer and fan to achieve a constant flow rate. The entire system was placed below an Aprovecho Portable Emissions Measurement System (PEMS) for evaluating the fuel combustion rate. The PEMS uses an HVAC blower and ductwork connected to a canopy to capture all of the emissions leaving the cookstove. A pitot tube "flow grid" was used to measure the net flow through the ductwork and thus the dilution rate of the stove emissions. A small sample of the diluted emissions was extracted from the duct for each run and directed through an enclosure

where the CO, CO_2 and PM concentrations are continuously analyzed thus providing a real-time measurement of the fuel combustion process. Knowing the CO/CO_2 concentrations gives the net carbon release rate which can be used to assess the combustion rate.

3.0.11 Calibration of the Forced Convection System

The anemometer in the forced convection system was calibrated by attaching a vacuum pump to the PVC pipe and maintaining various flow rates with a needle valve. The calibration process consisted of fixing the flow rate and reading the analog voltage output from the anemometer with the custom UPOD embedded system. Low flow rates were measured using a Gilibrator bubble meter, while large flow rates were measured using a flow totalizer. 3.1 shows an example of the calibration setup.

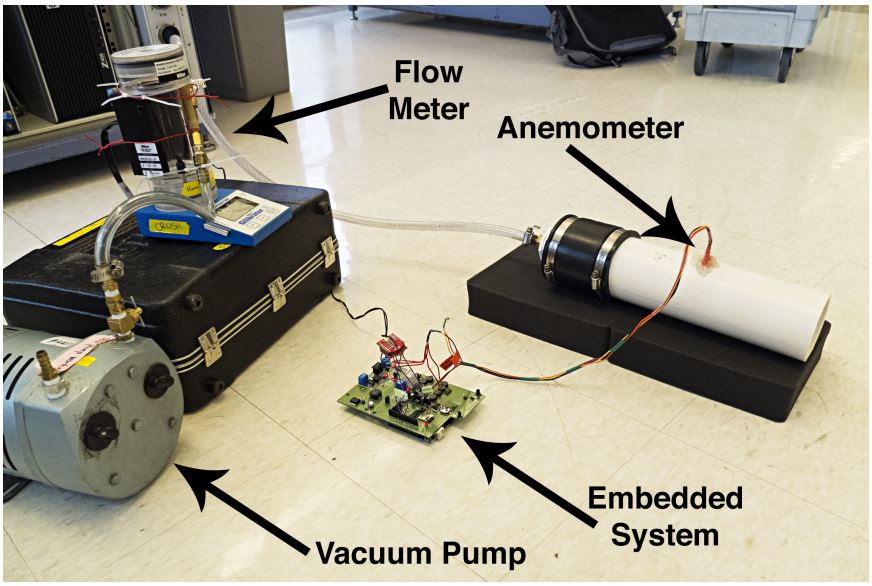

Figure 3.1: Anemometer Calibration Setup

A hot wire anemometer operates by measuring the heat transfer rate from a heated element under various flow conditions. The Modern Devices anemometer, specifically, measures the current necessary to maintain a heated semiconductor element at a constant temperature. If the thermal

conductivity of the fluid is constant, then the convective heat transfer coefficient increases quadratically with fluid velocity. In practice, the heat transfer rate requires knowing both this quadratic relation and the ambient temperature as well as parameters affecting the thermal conductivity of air, such as ambient pressure and humidity.

Change in anemometer output with respect to temperature were corrected for by repeating the calibration process in two rooms with different ambient temperatures. No correction was included for humidity or barometric pressure, which may constitute a significant source of error as anemometer calibrations were carried out in Boulder, Colorado (dry climate at 5000 feet ASL) whereas stove testing occurred in Seattle, Washington (humid climate at sea level). 3.2 shows the calibration curves generated in the two rooms with ambient temperatures of 21C and 26C, the upper set of data points being the calibration run in the cooler environment. The two fits per dataset show the difference between fitting the data using the flow velocity versus the digital output as the independent variable.

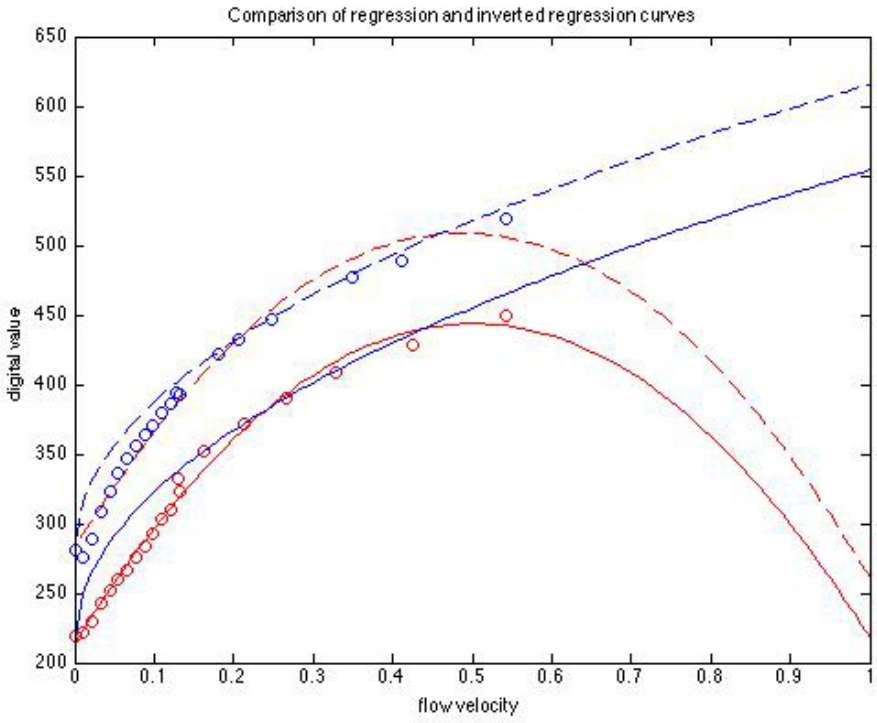

Figure 3.2: of Anemometer Calibration Curves

The forced convection system was completed by writing a custom code for the UPOD to control the fan speed for a desired input flow rate. This was achieved using a numerical PID feedback algorithm and pulse width modulation (PWM to vary the PWM value until the flow rate was within 5% of the desired flow rate. The actual flow rate was calculated by applying the anemometer calibration curve to the analog voltage output, and linearly interpolating between the curve for high and low temperature using the ambient room temperature.

3.0.12 Experimental Procedure

The experiments were carried out using one-inch cubes of Douglas fir as a sample fuel specimen. All samples were taken from one wood plank purchased at a local lumberyard. Samples were placed in an oven at 375 degrees Celsius for 2 hrs. to bring the fuel moisture content to a negligible level. A small hole was drilled in the bottom of the fuel samples such that the sample

could be placed on small wire stand on the fuel grade within the stove prototype. The wood grain was oriented parallel to the flow/flame-sheet direction.

3.3 shows the setup used for testing the fuel sample combustion runs.

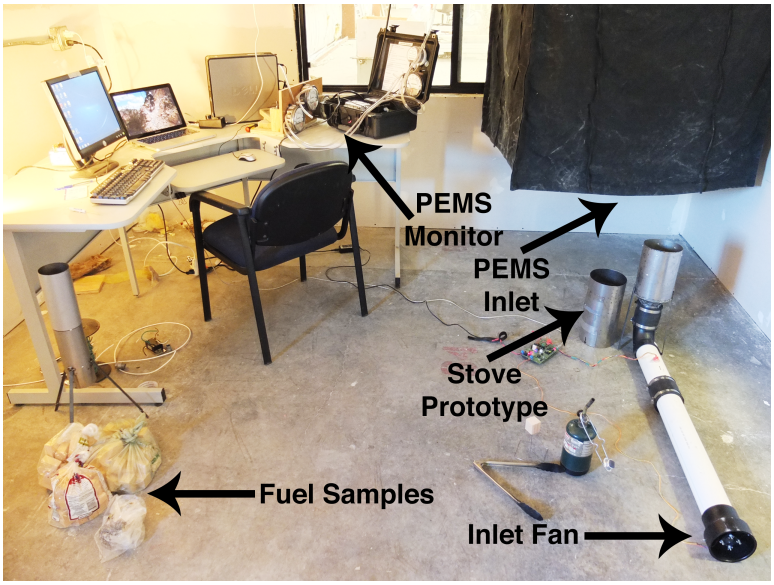

Figure 3.3: Experimental Setup

Each run consisted of setting the flow feedback for a constant flow rate. The discrete flow rates tested were {0.0125,0.025,0.05,0.1,0.15,0.225,0.35} m/s axial flow velocity (in a 6 inch diameter stove). A fuel sample was ignited by slowly rotating it on the wire stand while brushing over the surface with a blowtorch for approximately 10 seconds. The sample was then placed inside of the stove prototype and slid under the PEMS canopy. The sample emissions were measured until burnout.

This process was repeated for all of the flow rates with three replicates per flow rate. Three replicates were also conducted for a run without the forced convection system. The heat release rate from this run serves as the natural convection case used for validation of the methodology proposed in this work.

3.0.13 Assessing Heat of Combustion

The ultimate goal of the experiment is to correlate the heat release of a burning wood sample with the bulk fluid velocity within the combustion chamber. The experimental setup, however, does not directly measure ΔH_c° for the wood samples. Carbon emission rates (in the form of CO and CO_2) can be used to asses the heat release if ΔH_c° is known for the given wood type. Unfortunately the heat of combustion for wood is highly variable depending on the nature of pyrolysis, local temperature, etc. For example,ΔH_c° of alpha-cellulose, a main component of woody biomass, has been reported to be 54 kcal/mol using TGA[32] or 42 kcal/mol using isothermal pyrolysis [25]. It can be seen, then, that the actual heat of combustion of woody biomass can vary significantly depending on the nature of the combustion process.

This work takes a more general approach in which a wood type's net ΔH_c° is assessed using the ΔH_c° of its constituents. The relative composition of a wood sample affects the nature in which each of its constituents is pyrolyzed, but the error due to this affect is assumed to be of similar order as the variability in reported values of ΔH_c° for the sample as a whole.

Specifically, the net ΔH_c° of the woods sample can be calculated knowing the mol fraction of cellulose and lignin for the specific wood species. SERI[33] gives the heat of combustion for cellulose and lignin as 7250 Btu/lb and 11500 Btu/lb, respectively. Parker and Levan [30] give the wt % composition of Douglas fir as shown in 3.1. The average molecular weight of the constituents was used to compute the mol % of each constituent.

Table 3.1: Properties of Douglas Fir

type	MW [g/mol]	carbon	wt. %	mol %
cellulose	162	6	32.3	33.2
lignin	180	10	36.4	33.7
mannan	180	6	25.0	23.1
xylan	132	5	7.3	9.2

The net heat of combustion for Douglas fir can be calculated by adding the heat of combustion of the constituents scaled by their respective mol fraction. Here, the heat of combustion of mannan and xylan are taken to be the same as that of cellulose. Computing the net ΔH_c° and scaling by the average number of carbons for each constituent gives $\Delta H_c^\circ = 418 kJ/molC$. This heat release per mol carbon is used to calculate the rate of heat release of doulas fir using the measured rate of carbon emissions.

3.0.14 PEMS Performance and Calibration

The PEMS system operates by drawing the stove emissions into a small enclosure through a narrow sampling line several meters in length. The enclosure houses the gas sensors which read the pollutant concentration. The PEMS response characteristics can then be modeled as: 1) plug flow within the intake line and 2) a completely mixed flow reactor (CMFR) within the sensor enclosure.

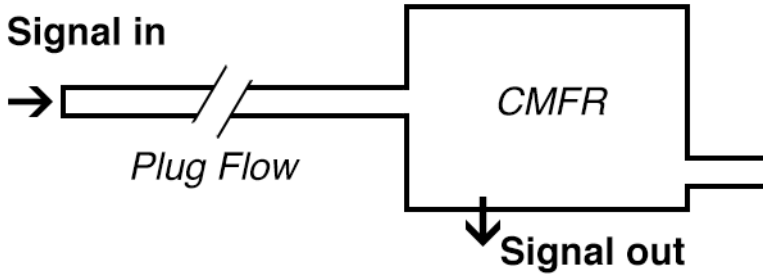

setup.png

Figure 3.4: Model within PEMS

The plug flow will introduce signal latency but does not affect the signal strength, where the signal is taken to be the sample pollutant concentration. The CMFR, however, is effectively a low-pass filter acting on the input signal. In other words, rapid changes in emissions are not captured with the PEMS system.

The response characteristics for the CMFR can be modeled if the flow rate through the PEMS

system and volume of the sensor enclosures are known. Neither of these was easily measurable on the PEMS system. An alternative method consists of placing a blowtorch under the PEMS intake canopy and measuring the CO_2 concentration. The blowtorch is meant to simulate a delta function input of CO_2.

The change in concentration within the enclosure for a CMFR model is given by:

$$\frac{dC}{dt} = \lambda \cdot (C_{in} - C) \tag{3.1}$$

where C is the concentration within the enclosure (output signal), C_{in} is the concentration entering the enclosure (input signal), and λ is the air exchange rate within the enclosure. Taking the Laplace transform of 3.1 gives the transfer function for the PEMS system as $\lambda/(s+\lambda)$ where λ is approximated given one-fifth of the time it takes to reach steady state. Equation 3.1 describes an exponential decay or growth when exposed to a delta input function.

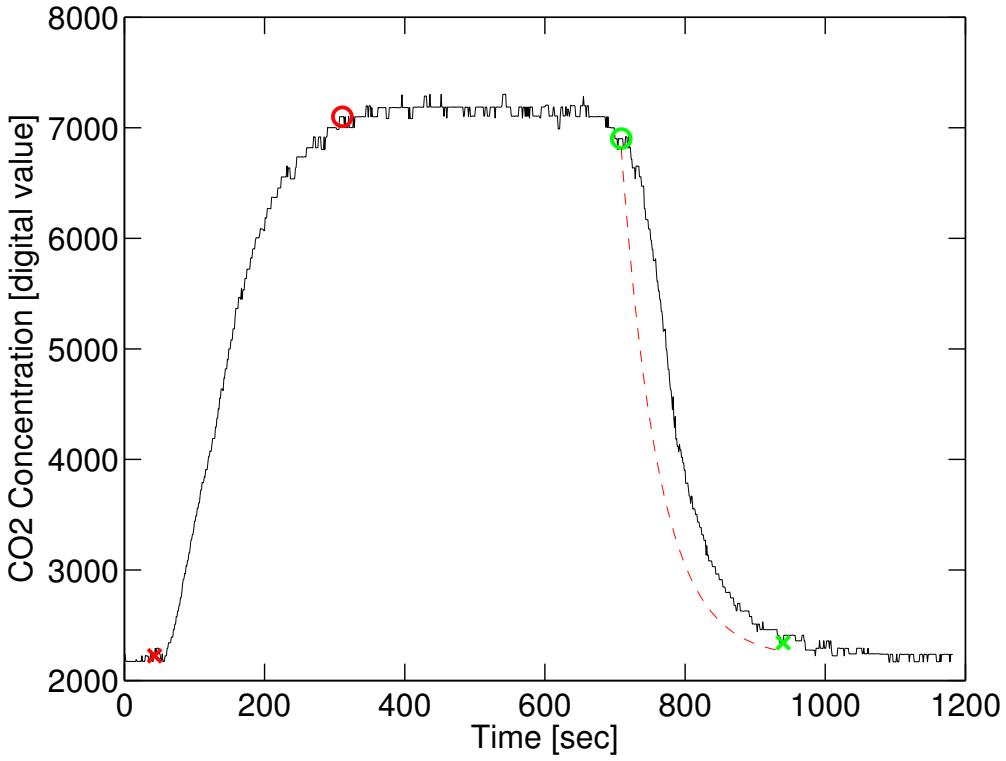

Figure 3.5: Reponse to Delta Input

3.5 shows the CO_2 measurement in the PEMS when exposed to the blowtorch delta input and the transfer function model fit to the growth and decay of the input signal. 3.6 is a Bode plot for the transfer function which describes the PEMS system. Attenuation frequencies for 10%, 3dB and 90% cutoffs are 0.01Hz, 0.07Hz and 0.19Hz respectively.

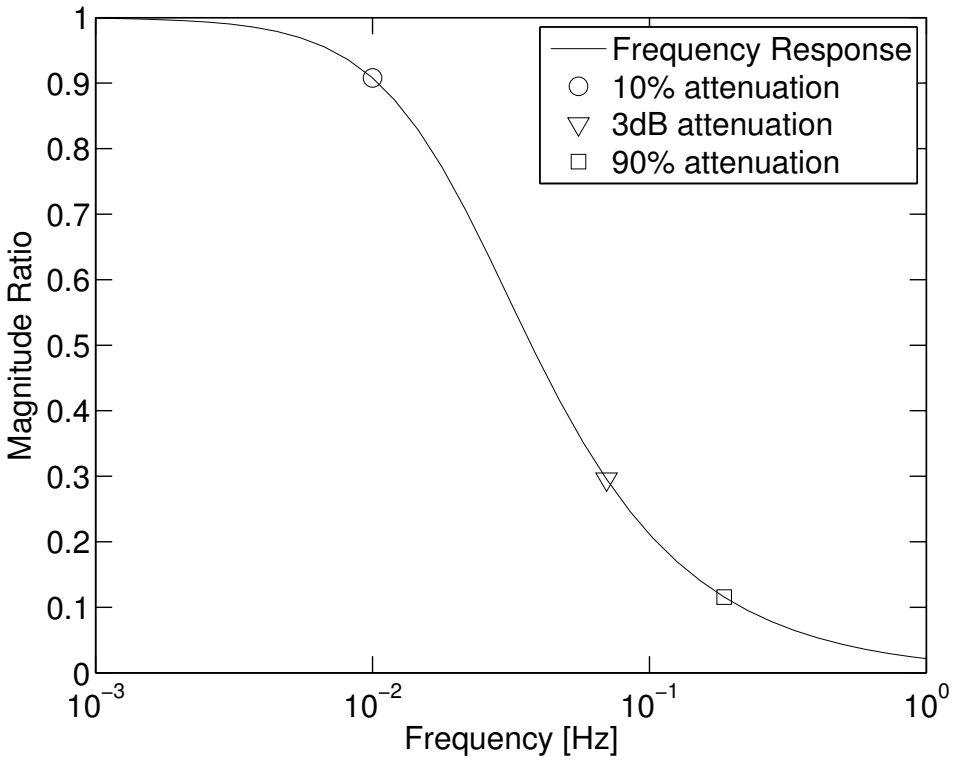

Figure 3.6: Bode Plot

From a physical perspective, the PEMS will poorly resolve signals with a characteristic time on the order of 14 seconds or faster. Changes in concentration must occur in periods under 100 seconds for no significant damping to occur.

Chapter 4

Stove Model

4.0.15 Setup

The stove prototype used in the experiment was modeled using the ANSYS 13.0 FLUENT computational fluid dynamics (CFD) software package. Recall that the objective of the model is to investigate the change in flow conditions with respect to a constant heat flux from the fuel surface. The goal then is not to push the fidelity of the computational model, rather to validate the method for decoupling the combustion process from bulk fluid flow proposed in this work.

The model setup consisted of an 8 inch long by 3-inch wide axisymmetric domain meant to simulate the full 6-inch diameter cylindrical combustion chamber. The inlet was sectioned into a 1 inch "fuel surface" and a 2 inch air inlet, while the opposite 3 inch surface serves as an air outlet.

Each section was given an appropriate boundary condition as outlined in 4.1

Table 4.1: Boundary Conditions for CFD Stove Model

surface ID	boundary condition type
inner wall	axis (axisymmetric)
fuel surface	constant heat flux
air inlet	pressure inlet
air outlet	pressure outlet
outer wall	adiabatic

The CFD solver used the incompressible laminar form of the Navier-Stokes equation with a Boussinesq approximation for buoyant driven flows. The Boussinesq approximation allows for small changes in density with respect to temperature (buoyancy) which are incorporated into a modified body force term: $f_i^* = -g\alpha(T - T_{ref})$. Here g is the acceleration due to gravity (defined in the x-direction given the geometry of this setup), α is the compressibility of the fluid, and $T - T_{ref}$ is the change in temperature of some point in the flow relative to a reference temperature. Values for the heat capacity (c_p) , the thermal conductivity (k) and the viscosity (μ) of air were taken to be those as standard temperature and pressure (STP).

4.0.16 Parameter Study

The CFD model was run for heat flux rates of {80,100,120,140.160,180,200} watts from the fuel surface boundary. 4.1 shows an example of the velocity contour solution with a heat flux of 140 watts from the fuel surface, while 4.2 shows the fluid velocity of every point in the mesh along the stove air outlet.

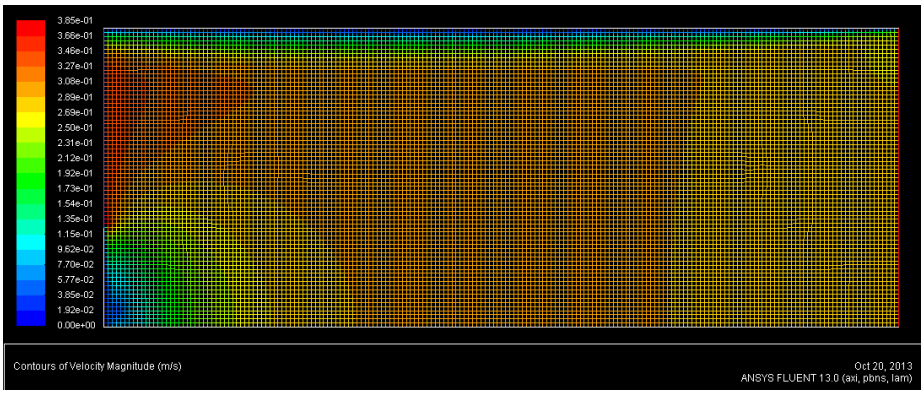

Figure 4.1: Contour at 140W Flux from Fuel Surface

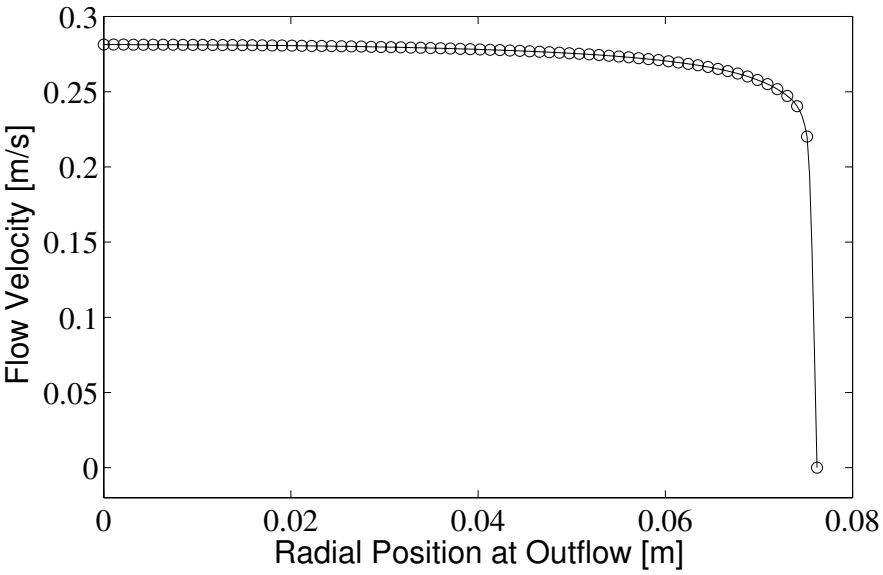

Figure 4.2: Profile at Outlet with 140W Flux

The flow velocities at every point in the mesh across the air outlet were averages to give a bulk flow velocity for each heat flux case.

Chapter 5

Cookstove Results

5.0.17 Experimental Results

The PEMS system measured the emissions for each sample run in this experiment. The heat of combustion for the fuel sample was assessed at the emissions rate measured when the fuel sample burning process reached steady state. This was taken to be the plateau region in the middle of the emissions time series. 5.1 shows an example of the CO_2 emissions measured from a fuel sample burning in the stove prototype with an axial flow velocity of 0.05 m/s.

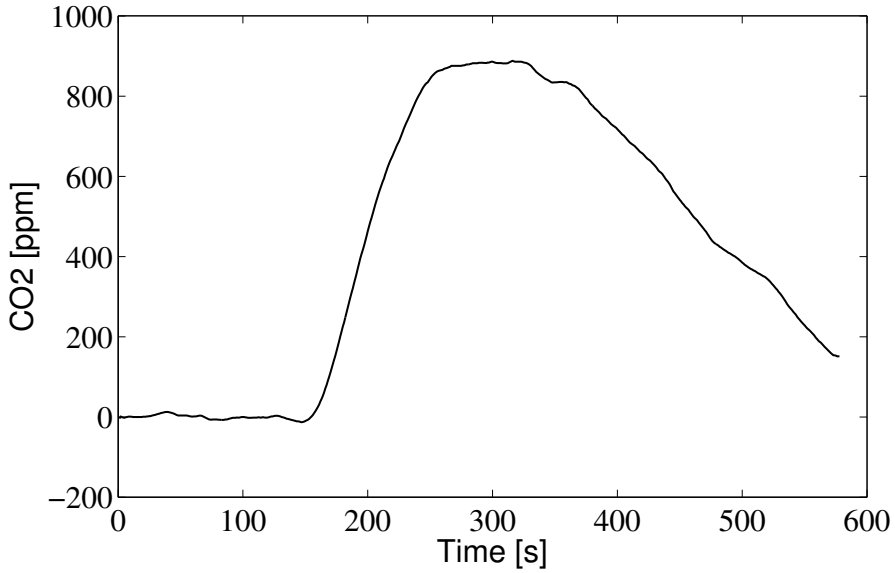

Figure 5.1: CO_2 emissions at 0.05 m/s flow velocity

The HVAC blower dilution rate and the emissions concentrations were used to calculate the net carbon release rate from the burning samples. Applying the heat of combustion determined for Douglas Fir gives the average heat release rate for a given forced air flow rate.

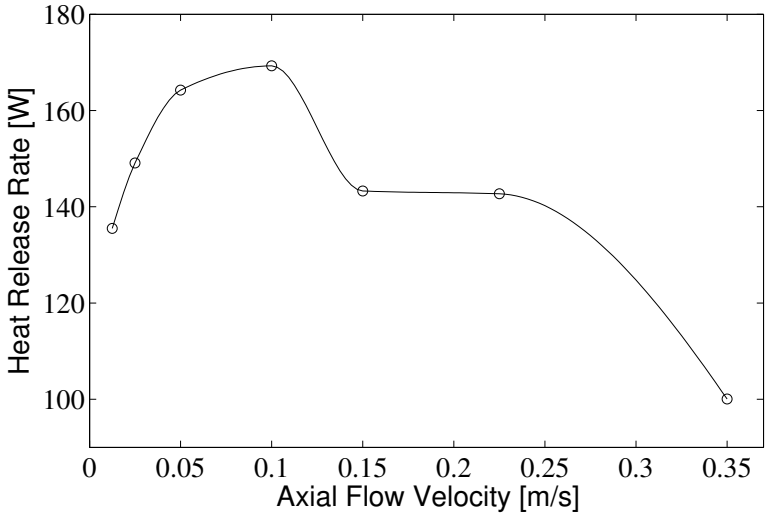

Figure 5.2: Heat Release Rate as a Function of Axial Flow Velocity

5.2 shows the average measured heat release of the fuel samples with respect to axial flow velocity. Data points represent the mean value of the three replicates for each flow velocity.

5.0.18 Modeling Results

Mean flow velocities were acquired for each heat flux value chosen in the CFD stove model parameter study. The means were calculated using the flow velocity at each node across the stove outlet.

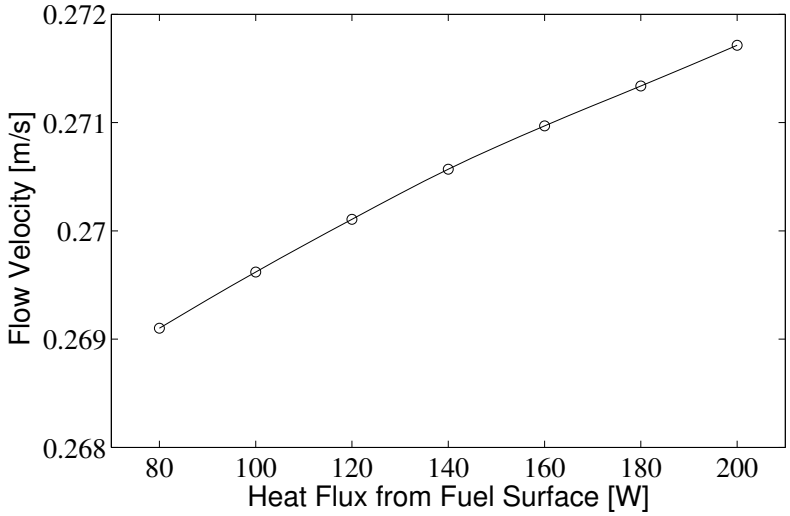

Figure 5.3: Flow Velocities versus Heat Flux from Fuel Surface

5.3 shows the resulting mean axial flow velocity for the various heat flux values.

5.0.19 Overall Results and Discussion

5.4 shows the experimentally derived results against the modeled results. The intersection of both curves signifies the point at which one would expect natural convection to occur. That is, at the point of intersection, one cannot discern between flow causing the heating rate and the heating rate causing the flow. This is where the feedback between flow and heating rate find their equilibrium in the natural convection case.

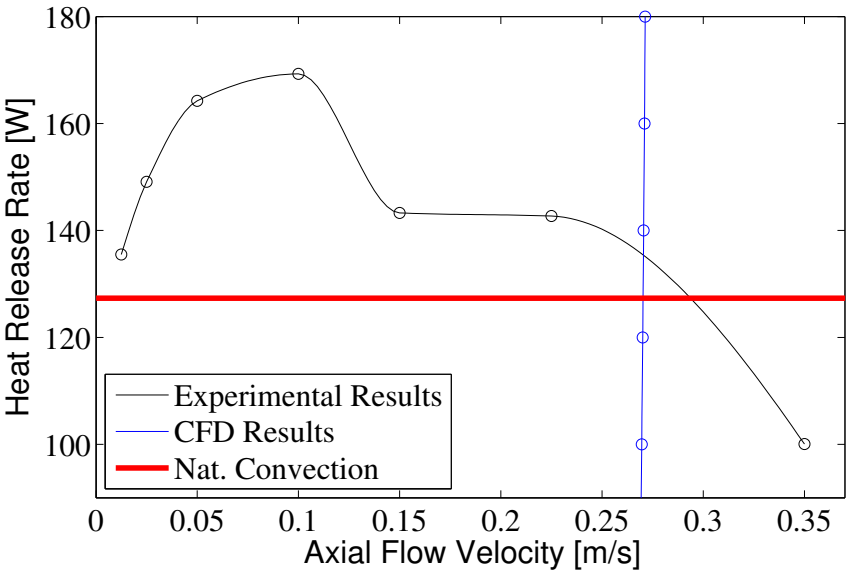

Figure 5.4: of Forced Convection Measurements with Buoyant Flow Model

The red line shows the measured heat release rate for natural convection, which falls below the heat release rate theoretically anticipated by the intersection of the experimental and modeled data. Overall, however, the theoretical heat release is close enough in proximity to the observed heat release to justify the validity of this approach. It should be noted that the exact intersection of the experimental and modeled cases depends on the interpolation of experimental data between the 6^{th} and 7^{th} data points. A linear interpolation would better approximate the natural convection case instead of the smoothed regression in 5.4.

Gross approximations in the model case may also contribute to the discrepancy between observed and modeled heat flux rates. For example, 5.5 shows the temperature contour solution with a heat flux of 140 watts from the fuel surface.

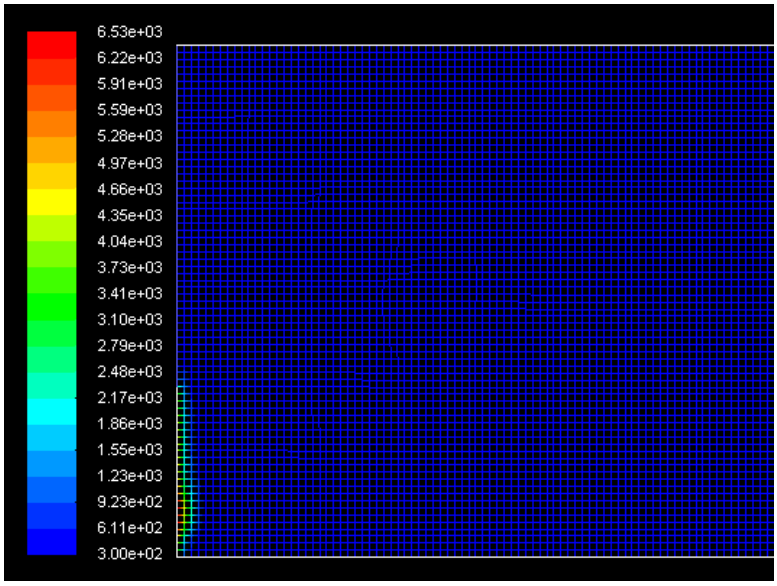

Figure 5.5: Countour at 140W Flux from Fuel Surface

In reality, the highly heated region extends further from the fuel surface due to the advection of pyrolyzed fuel and the residence time necessary for the combustion process. A mixture fraction approximation is a suitable method for attaining better spatial fidelity with respect to flame sheet position without compromising the simplicity and efficiency needed for practical stove modeling and design.

Other potential sources of error include the low pass response nature of the PEMS system and uncertainty in the calibrated output from the anemometer. An upward shift in the measured heat release rate can be expected when the time period for the steady-state plateau observed during the burn case is of the same order as the characteristic time for PEMS damping. In most cases of the experiment, however, the steady state burn time (e.g. 5.1 significantly exceeded the minimum time necessary to prevent physical signal attenuation from mixing in the PEMS system). As such, the PEMS response time should not be considered a significant source of error in the experimental measurements.

The anemometer, however, was only calibrated for changes in ambient temperature (see 3.0.11). The calibration did not include compensation for changes in ambient humidity or baro-

metric pressure. It can be assumed that the humidity and pressure are consistently higher in Seattle, WA, where the experimental data was collected, versus Boulder, CO, where calibration took place. Higher pressure and humidity would both increase the thermal conductivity of the working fluid (ambient air) running over the hot wire anemometer. As such, the heat transfer (and signal output) from the anemometer in Seattle, WA would be consistently higher for a given flow rate and ambient temperature. This would positively bias the computed flow rates. This is a notable source of error, and it can be seen that a leftward shift in the experimental data of 5.4 would result in better agreement between the experimental/model coupling and the natural convection case.

5.0.20 Sources of Error in Implementation and Future Work

The test case does well to validate the methodology presented in this work. It is important, however, to outline underlying assumptions and possible sources of error when applying this methodology to practical design scenarios.

First and foremost, this case was developed using wood of a specific type, size and moisture content. It is evident that these three parameters significantly affect the nature of the experimentally derived relationship between heat release and bulk flow rate. In practice, the experimental procedure of correlating heat release with flow rate would need to be carried out for all combinations of pertinent factors. Some simplifications may still apply making this full-factorial process less tedious, such as a weighted scaling of heat output with biomass specific area.

Secondly, the experimental data collected in this work did not consider the interaction of combustion and heating of the stove walls. The fuel sample used in this experiment was small enough with respect to the model stove diameter (1 inch versus 6 inches), that no significant heating was observed in the stove walls. This is supported by experimental observation in which the steel stove model did not heat up significantly above ambient temperature, and in the CFD model in which temperature gradients are negligible in the vicinity of the wall boundary.

In practice, the stove walls cannot be assumed to be adiabatic as significant conjugate heat

transfer occurs between the heated fluid and the solid walls (although it is advantageous to make the walls of low thermal mass and highly insulating material [11]). This must be taken into account when applying the experimentally derived correlation to modeled cases. Luckily, it does appear from the simulated CFD case (see 5.3) that the resulting flow velocity does not depend significantly on the fluid heating rate spanned in the parameter study. This implies that the resulting flow velocity is more significantly affected by the stove geometry and resistance to flow.

It follows that knowing the heat release rate in the model case is more significant for determining efficiency and heat transfer characteristics than it is for determining the bulk flow rate. As such, it stands to reason that empirical correlations should be collecting using a instrumentation setup where the combustion process is far from the stove wall (thus mitigating thermal gradients and making the wall as adiabatic as possible). This would result in a correlation entirely independent of stove wall effects (neglecting radiation) and only a function of flow velocity. Strong results can be expected when coupling this with a CFD model including wall heat transfer affects.

5.0.21 Conclusions from Empirical-Model Coupling Method

Overall, the method of using empirically derived relationships between flow rate and heat release rate to validate CFD models does well to anticipate the actual operating conditions of natural draft biomass cookstoves. As previously mentioned, the experimental procedure here developed would need to be repeated across the parameter space of fuel type, moisture content, etc...

In practice, a natural draft stove designer could model the stove performance with a variety of heating rates. Cross-referencing the bulk flow and heating rates with tabulated experimental data could inform him/her as to case which is most likely in operation. The thermal efficiency/performance characteristics of this most likely case could then be compared with similar cases for other geometries. The best performer would be that selected for prototyping and, perhaps, production.

The practicality of this method requires further investigation. The tedious process of repeating the experiment for different fuel factor combinations and the uncertainty due to fuel variability

and user habits may not justify the benefits gained in operating condition fidelity. These experiments, however, need only be carried out once, and can be implemented in all future stove modeling work.

Chapter 6

Inexpensive Pollutant Sensing Technology

6.0.22 Introduction

The use of inexpensive sensor networks and embedded systems [24] is quickly emerging as a key player in the monitoring of local and regional air quality. In particular, these technologies make pollutant monitoring accessable to researchers assessing personal exposure and health affects as outlined in 1.0.4. The use of inexpensive sensors, however, requires significant post-processing and interpretation of sensor signals. This work addresses the derivation of a quantification model for Metal Oxide Type (MOx) sensors.

6.0.23 Metal Oxide Type Sensors

MOx sensors [26] are one of several technologies being used in sensing gas phase pollutants. Many varieties of MOx sensors exist for the detection of different gas species. All types, however, function in a similar manner. An oxidation or reduction reaction occurs when species bind to the sensor surface resulting in the removal or injection of free electrical charge into the semiconductor material [17]. This process changes the sensor's electrical conductivity, which is measured by external instrumentation.

Unfortunately there are many challenges when trying to quantify the sensor response. All MOx sensors suffer from significant interference effects with temperature, humidity[7] and other gas species. Even when these parameters are controlled, the sensor conductivity is highly non-linear with respect to the gas species of interest. Most MOx sensors also exhibit 'out-of-the-box'

variability from the manufacturing process. Finally, sensor signals will also drift over time from both poisoning (permanent bonding to the sensor surface) and changes in the sensor's heating element resistance caused by thermal stress.

Many approaches exist for the quantification of metal oxide gas sensor, yet most practical models are based entirely on experimentation and a postereori knowledge of sensor behavior [3][19]. While these models provide acceptable results, they tend to be specific to sensor type and operating conditions. It would be advantageous to use a model derived entirely from the theory of chemistry and semiconductor physics, yet in practice this proves prohibitively complex. The approach presented here is rooted in the principles of semiconductor science, yet uses experimental observations to make informed assumptions and simplifications. Doing so retains some physical insight as to sensor behavior, yet allows the model to be tailored to sensor specific applications and proves to be effective in real-world implementation.

The model derivation process consisted of lab experimentation and ambient colocation measurements. The theoretically derived model was first applied to experimental data, using the Sensortech (formerly e2v) MICS-5525 as an example of a commercially available MOx type carbon monoxide sensor. In practice, sensors are employed in low pollutant concentration (low detection limit) environments with significant environmental variability, hence the need to properly address temperature affects. Humidity effects were neglected as they are at least an order less significant than temperature effects, particularly for CO sensors[18].

MOx sensors are operated at elevated temperatures in order to facilitate the surface chemistry reactions of interest. Most commercially available MOx sensors have built in heating elements to keep the sensor surface in the vicinity of a target temperature. The resistance of the heating element and thus the heat output tend to change over time. This complicates the ambient temperature correction term as the relationship between surfaces temperature and ambient temperature is not constant when the heater output varies over time. To correct for this drift effect, the heater resistance was measured over several months and incorporated into the model as a temporally varying temperature correction term. No drift due to poisoning was incorporated in the model, as

drift of this type can only be accounted for by using periodic calibrations.

The sensors were then collocated with a reference carbon monoxide instrument in an urban environment. An optimization algorithm was used to dynamically fit the reference data to the model prediction, thus modifying the model parameters determined in lab experimentation.

6.0.24 Principles of MOx Operation

Barsan and Weimar [8] present and in-depth discussion of the metal oxide semiconductor conduction model in which a sensor's conductivity is analytically attributed to changes in gas-phase species concentrations. Solving for the conductivity entirely from theory, however, requires extensive knowledge of the chemical kinetics and semiconductor electrical properties. Even if all parameters are known, the functional relationship between conductivity and ambient gas concentration requires numerically solving a complex system of several non-linear relations. Doing so is not practical in many applications. It is thus necessary to incorporate extensive simplifications and experimental data in the model derivation.

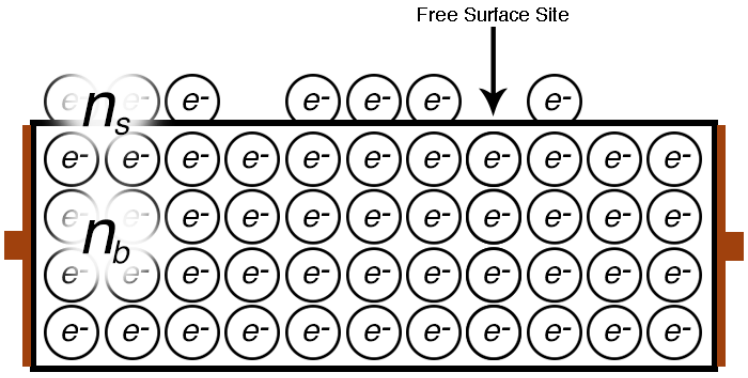

Figure 6.1: sensor without surface reaction

First consider the general principles driving MOx sensor operation. 6.1 is a simplistic representation of a MOx sensor element in an environment void of surface reactions. Pertinent attributes

of the MOx element include the free charge density in the bulk material volume (charge which is free to conduct across the material), and the surface charge density (charge on the surface of the MOx sensor, which is free to react with reducing agents). The surface charge density will change with temperature.

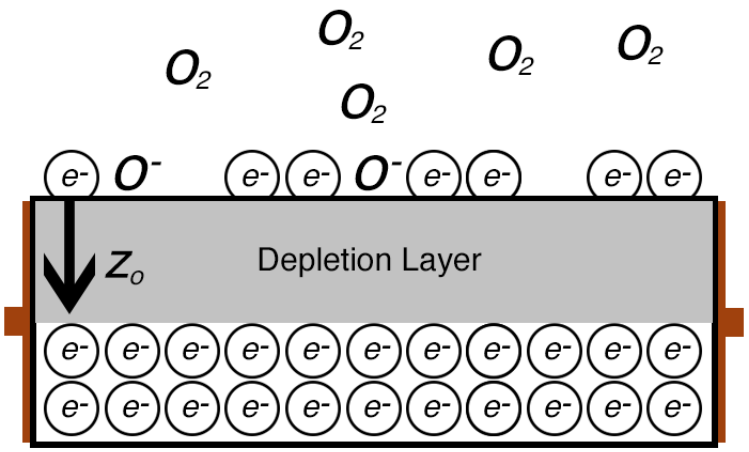

Figure 6.2: sensor with surface reaction

Surface electrons are added or removed from the surface when the MOx sensor is exposed to reacting species (6.2). Chemical reaction theory governs these reactions. When charge is removed from the MOx surface, the bulk semiconductor responds by restoring some of the surface charge from the bulk charge 'reservoir'. This results in "band bending" and depletion of some of the bulk charge within the semiconductor volume. It can then be seen that the surface charge provides the physical coupling between the semiconductor physics and the gas-phase surface chemistry.

Net conduction of electrons within the MOx element occurs parallel to the sensor surface, whereas the depletion of charge occurs normal to the surface. It stands to reason then that the conductivity (or resistance) of the MOx sensor is a function of the depletion depth of charge within the bulk semiconductor.

Other important factors include the surface site concentration of chemisorbed species, the temperature dependence of chemical reactions and semiconductor band-bending and the nature of

intermediate and global reaction mechanisms. In this derivation, chemical reaction mechanisms are mostly neglected or generalized while temperature effects are more rigorously accounted for.

6.0.25 Model Derivation

A practical model can be generated by applying practical simplifications to the theoretical derivation a of MOx sensor model. Simplifications are motivated by a desire to have a closed-form, easily manipulated algebraic equation relating measurable quantities (resistance, ambient air temperature, etc...) with the concentration of target pollutants. The focus here is on low detection limits where the sensor surface is far from being saturated with the target pollutant. The strong dependence of the sensor signal on sensor surface temperature (thus also ambient temperature) suggests the need for good fidelity between the final equation's temperature term and the governing equations driving the temperature affect.

To begin, it is assumed that the metal oxide semiconductor material is fabricated as a compact layer impermeable to gas-phase species. The metal-oxide crystals thus have tight grain boundaries with uniform imperfections over the volume of the sensing region. This supports the assertion that bulk charge transport (current in the sensor) traverses parallel to the sensor surface, whereas charge depletion due to surface reactions occurs normal to the semiconductor surface.

The conductivity of the semiconductor will depend on the depletion layer depth and the decrease in free charge density. Following Barsan and Weimar's derivation, the charge removed from the depletion layer is taken to be equal to the charge captured by chemisorbed species at the semiconductors surface. This is known as the electroneutrality equation in the Shottky approximation and is given by 6.1 where ϕ is the species' ionization form, n_b is the bulk charge density in the semiconductor material and z_o is the depletion layer thickness normal to semiconductor surface. The bulk charge density n_b is assumed constant under steady operating conditions. Θ is the surface site coverage of chemisorbed species, which is defined as the sum of all occupied sites over the total surface site concentration, $[S_t]$ over which gas-phase species compete.

$$\phi \cdot \Theta \cdot [S_t] = n_b \cdot z_0 \tag{6.1}$$

If, as the electroneutrality equation suggests, the depletion layer is void of all free charge carriers, then only the bulk charge n_b in the non-depleted layer contributes to the semiconductor conductivity. Here the conductance, G_s is taken to be proportional to the non-depleted region and scaled by a characteristic length, L. The characteristic length is sensor specific, which in part explains inter-sensor variability as a product of inconsistencies in sensor manufacturing.

$$G_s = \gamma \cdot \ n_b \cdot L \cdot (h - z_o) \tag{6.2}$$

Here h is the semiconductor thickness and γ is an unknown constant of proportionality.

Calculating the surface site coverage Θ in 6.1 requires extensive knowledge of the reaction mechanisms and chemical properties governing surface and gas phase reactions. A simplified form assumes atmospheric gas phase reactants to bind directly with free surface electrons on the sensor surface:

$$S + \alpha \cdot e^- + C_{(g)} \rightleftharpoons C_{(s)}^{-\alpha} \tag{6.3}$$

where S is the number of unoccupied sites, e^- are free surface electrons whose concentration is herein after denoted $[n_s]$ and $C_{(g)}, C_{(s)}$ are gas phase and chemisorbed reactants, respectively. If the surface sites are predominantly occupied by one gas phase reactant (typically oxygen), and it is assumed that $\Theta << 1$, then 6.3 gives:

$$\Theta = \frac{k_f}{k_r} \cdot [C_{(g)}] \cdot [n_s] \tag{6.4}$$

where k_f and k_r are the forward and reverse rate constants, respectively, and it is further assumed that the reaction is of first order in its reactants. The rate constant is given by the Arrhenius rate equation:

$$k = A \cdot exp\left(-\frac{E_a}{k_B T}\right) \tag{6.5}$$

where E_a is the reaction activation energy, k_B is the Boltzmann constant, and T is the semiconductor temperature.

Combining 6.1 with 6.4 and assuming that the reactants are singly ionized, gives:

$$z_o = \frac{[S_t]}{n_b} \cdot \frac{k_f}{k_r} \cdot [C_{(g)}] \cdot [n_s] \tag{6.6}$$

The surface charge density n_s is related to the semiconductor band bending qVs and, similar to the Arrhenius equation, is given by:

$$n_s = n_b \cdot exp\left(-\frac{qV_s}{k_B T}\right) \tag{6.7}$$

The surface band bending can be calculated as per Barsen and Weimar[8] by solving the Poisson equation, giving:

$$qV_s = \frac{q^2 \cdot n_b}{2 \cdot \epsilon \cdot \epsilon_0} \cdot z_0^2 \tag{6.8}$$

Simplifying 6.8 assumes the band bending to vary linearly rather than quadratic ally with z_o, allowing qVs to be expressed as:

$$qV_s = -\xi \cdot z_o \tag{6.9}$$

where ξ is a proportionality constant.

Combining 6.6 with 6.7 and 6.9 allow z_o to be expressed as:

$$z_o = [S_t] \cdot \frac{k_f}{k_r} \cdot [C_{(g)}] \cdot \exp\left(\frac{\xi z_o}{k_B T}\right) \tag{6.10}$$

A closed form solution using the Lambert W function gives z_o as:

$$z_o = -\frac{k_B T}{\xi} \cdot W\left([S_t] \cdot \frac{k_f}{k_r} \cdot [C_{(g)}] \cdot \frac{\xi}{k_B T}\right) \tag{6.11}$$

Unfortunately the Lambert W function is ill-suited for algebraic manipulation and general model implementation. In practice, the unknown coefficients are determined experimentally, so

one need only be concerned with preserving model form and modes of non-linearity. It was found that an exponential function would suffice in lieu of the Lambert W function. That is, there exists coefficients $\{a, b\}$ such that $aexp(bx)$ adequately captures the non-linearity in $W(cx)$ over some range of interest $\{x_1, x_2\}$. The physical meaing in the constant coefficient values is lost when $c \rightarrow \{a, b\}$. Combining the above approximation with 6.11, 6.2 and 6.5, allows for the conductance to be written as a function of temperature and atmospheric reactant concentration as:

$$G_s/L = a_1 - a_2 \cdot T \cdot exp\left(\frac{a_3 \cdot [C_{(g)}]}{T^2}\right) \tag{6.12}$$

For a carbon monoxide (CO) sensor, CO acts as a reducing agent, binding to oxygen groups already chemisorbed to the surface. The result is to return free charges to the semiconductor previously removed by the oxygen bonds. Barsan and Weimar [8] present a rigorously derived closed form solution for conductivity as a function of ambient CO partial pressure. Here, however, we will make use the simplified conductivity equation 6.12 and allow $[C_{(g)}] \rightarrow a_4 + a_5 \cdot [CO]$. In this case, a_4 is a proxy for chemisorbed oxygen and a_5 describes a linear propensity for CO to remove the chemisorbed oxygen. The surface sites occupied by oxygen are assumed to be constant, any change due to atmospheric variability being negligible relative to the CO effect.

The final model gives free parameters to all unknown constants. The values of the constants are determined experimentally, and can generally characterize the behavior of all sensors of a given type after accounting for inter-sensor variability. The validity of the above assumptions are investigated in experimental observation.

6.0.26 Experimental Setup

An array of three Sensortech (formerly e2v) MICS-5525 carbon monoxide sensors were placed in an aluminum enclosure and attached to an inlet mixing manifold. Three mass flow controllers (MFCs), controlled by a LabView VI, fed dry air, humid air and a 1000ppm carbon monoxide (CO) gas standard into the mixing manifold to achieve six levels of CO concentration between zero and 2.8ppm. A heat lamp was duty cycled by the LabView VI to ramp ambient gas temperature

within the enclosure from approximately 298K to 315K. A given sample run consisted of holding the inlet CO concentration and absolute humidity constant while cycling through different temperature levels. The three sensor signals were collected at a 1 Hz frequency using a LabJack 10 bit analog-to-digital converter, and the temperature and relative humidity was recorded using a Sensirion SHT-11 RhT sensor.

6.0.27 Experimental Results and Parameter Estimation

Sensor resistances were acquired for each sensor at various temperature levels for six runs at concentrations of {0, 0.6, 0.9, 1.5, 2.3, 2.8} ppm carbon monoxide. Absolute humidity was held at 0.015 [mol/mol] (equiv. 40%Rh at 25C) for all runs.

The response of the MICS-5525 sensor, as shown in 6.3, was close to linear in temperature over all concentration levels.

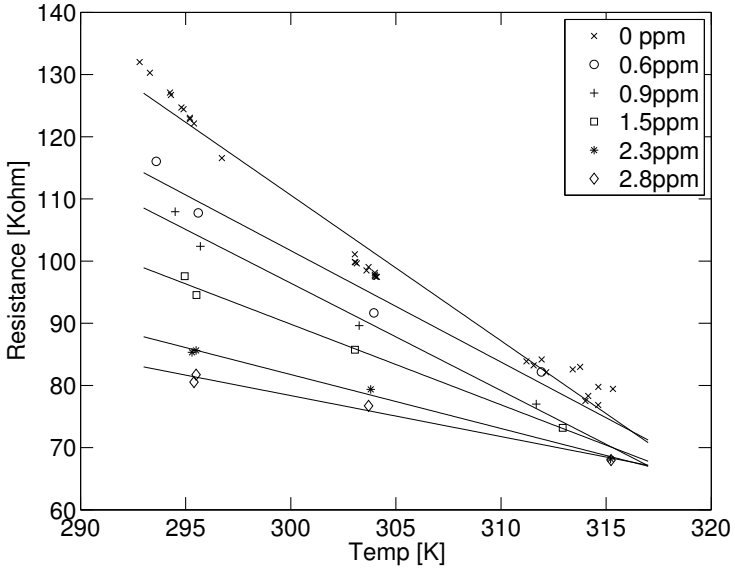

Figure 6.3: MICS-5525 Response to Temperature at Various CO Concentrations

It is common practice to normalize the signal resistance by a sensor-specific constant value. Doing so helps to account for inter-sensor variability as shown in 6.4, the physical basis of which is previously discussed in the derivation of 6.2.

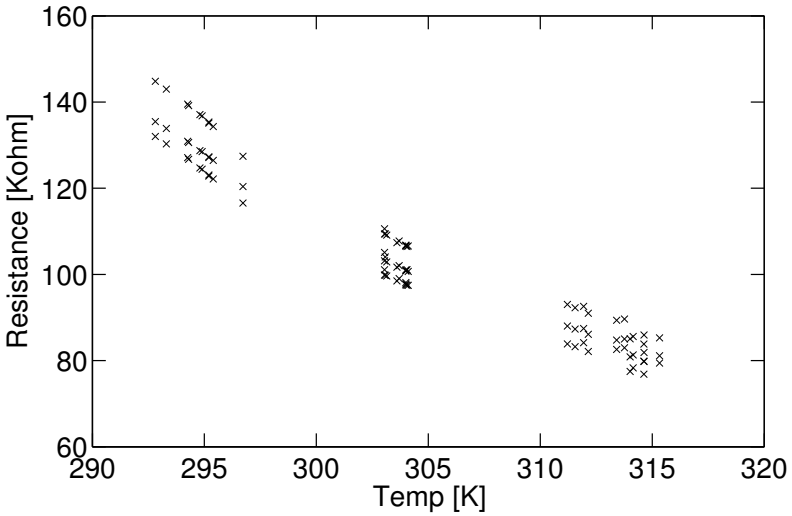

Figure 6.4: MICS-5525 Inter-sensor Variability for Three Sensors at Zero Concentration

Each sensor was given a resistance values, R_o, defined as the resistance of the sensor at 298K in zero air. These values were taken from the linear regression of resistance versus temperature at zero concentration for each of the three sensors. Normalizing each sensors' resistance by its R_o value gives good inter-sensor agreement as seen in 6.5.

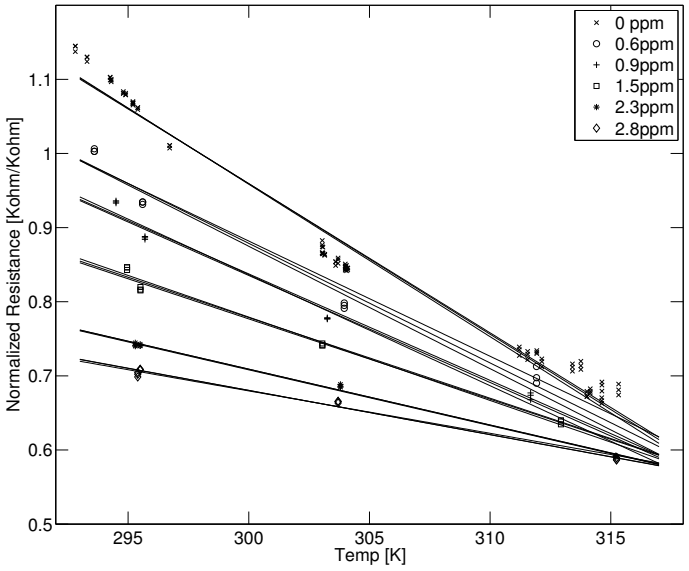

Figure 6.5: MICS-5525 Normalized Response for Three Sensors

The measured resistance,R_s, is related to the derived conductivity model 6.12 by the reciprocal relationship $\sigma = \rho^{-1}$ between conductivity and resistivity respectively. It was found that neglecting the hyperbolic term and taking conductivity to decrease proportionally to resistivity provided sufficient results. Then linearizing 6.12 with respect to temperature at 298K based on obervations in 6.3 gives the model form used for the MICS-5525 sensor:

$$R_s = (p_1 + p_2 \cdot [CO]) \cdot exp(p_3 \cdot [CO]) \cdot (T - 298) + p_4 \cdot exp(p_5 \cdot [CO]) + p_6 \tag{6.13}$$

The slope and pseudo-intercept (defined as the normalized resistance at 298K) were taken from each sensors' linear regression at each concentration level. The slope term, $(p_1 + p_2 \cdot [CO]) \cdot exp(p_3 \cdot [CO])$, and the pseudo-intercept term, $p_4 \cdot exp(p_5 \cdot [CO]) + p_6$, where then fit to the experimental data using a least-square approach as shown in 6.6 and 6.7.

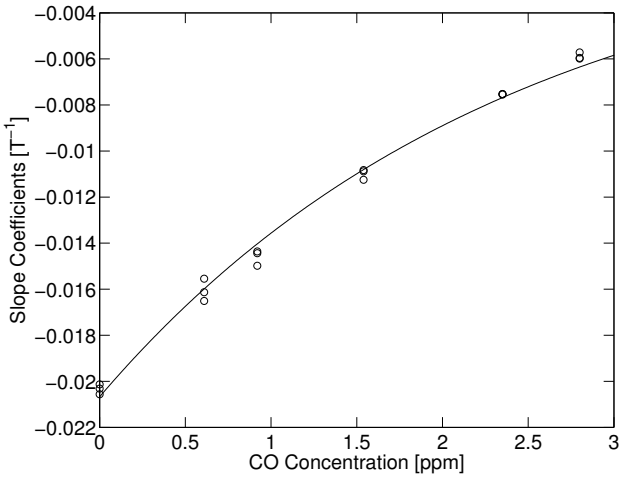

Figure 6.6: MICS-5525 Temperature Slope Coefficients

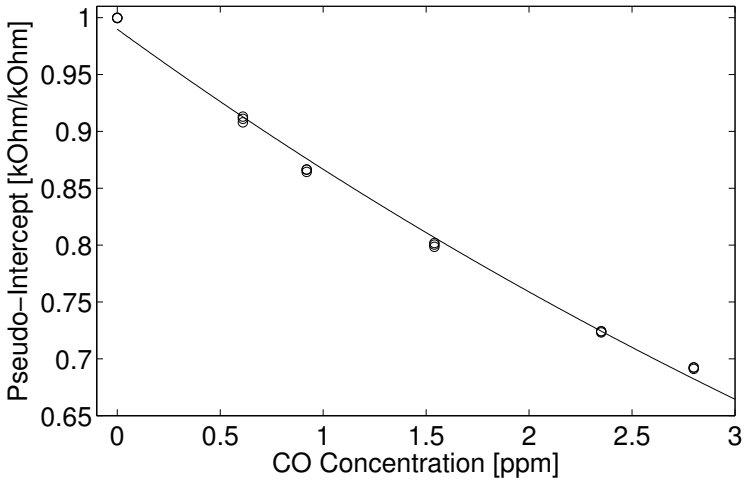

Figure 6.7: MICS-5525 Temperature pseudo-Intercept Coefficients

The parameters generated in the lab experiment predict CO concentration well under lab conditions, yet still present difficulties when implemented in real-world applications.

6.0.28 Sensor Heater Drift

It can be seen from the previous section that temperature plays a significant role in the sensor output and must be compensated for in any MOx quantification model. Many MOx sensors also exhibit heater drift in which the resistance of the heating element in the sensor will drift over time. When the heater resistance changes so too does the heater power output and thus the sensor surface temperature.

The ambient air temperature is directly related to the sensor surface temperature by the convective heat transfer equation: 2

$$Q(t) = h_t \cdot (T_s - T_a) \tag{6.14}$$

where T_s is the sensor surface temperature, $T_a$is the ambient temperature, $Q(t)$ is the time varying sensor heater output and h_t is the convective heat transfer coefficient. When $Q(t)$ and h_t do not change, the ambient temperature scales directly with the surface temperature. It is assumed that h_t is constant under steady ambient air flow (e.g. a constant flow of air over the sensor from an

inlet fan).

The power output from the heater resistor is a function of the heater resistance, $R_h(t)$, and the voltage drop across the resistor, $V_h(t)$, given by:

$$Q(t) = \frac{V_h^2(t)}{R_h(t)} \tag{6.15}$$

The voltage drop across the resistor depends on the excitation voltage, V, and the voltage divider resistor value, R_{hd}, given by:

$$V_h(t) = V \cdot \frac{R_h(t)}{R_h(t) + R_{hd}(t)} \tag{6.16}$$

The change in heater resistance for four MICS-5525 sensors were measured over a 250+ day period. The resistance was consistent across the four sensors, the difference in heater resistance being within the measurement error. The drift in heater resistance over time for one sensor is shown in 6.8. Note that the discrete steps in resistance are due to the sampling resolution, and intermediate data points being due to the daily averaging process.

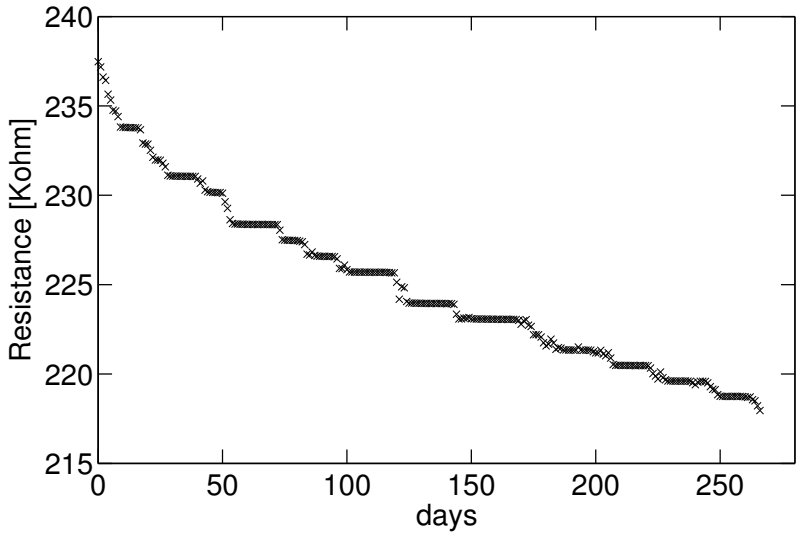

Figure 6.8: MICS-5525 Heater Resistance Drift over Time

A second order polynomial of the form:

$$R_h(t) = a_1 + a_2 \cdot t + a_3 \cdot t^2 \tag{6.17}$$

was fit to the heater resistance data.

$Q(t)$ is then given by 6.15, 6.16 and 6.17.

Equation 6.18 can be rewritten:

$$Q_o = h_t \cdot (T_s - T_a + \Delta Q_h / h_t) \tag{6.18}$$

allowing the chance in heater output ΔQ_h, where $\Delta Q_h = Q_h(t) - Q_h(0)$, to manifest itself as a correction to the ambient temperature measurement:

$$T_a^* = T_a - \frac{\Delta Q_h}{h_t} \tag{6.19}$$

Equation 6.19 gives a modified temperature term when $T \rightarrow T_a^*$ in the sensor resistance model 6.13. Note that the convective heat transfer coefficient is unknown and must be determined experimentally.

6.0.29 Colocation Setup

Two UPOD embedded system platforms were each outfitted with 4 MICS-5525 CO sensors and collocated with a Thermo Scientific Model 48 reference instruments at the CDPHE CAMP site. The monitoring station is located at a busy intersection in downtown Denver at 2105 Broadway St. The monitoring station is adjacent to a busy motorway resulting in good pollutant concetrations during rush hour periods. The reference instrument provided a dynamic concentration reading for the examination of discrepancies between sensor operation in the lab and in the field. The UPODs were placed near the reference instrument inlet on the roof of the monitoring station. The temperature and humidity was also measured in the UPOD system enclosure. The sensor resistances, relative humidity and temperature were sampled at 0.3Hz and averaged over one minute periods.

6.0.30 Colocation Results and Parameter Optimization

The UPODs were collocated at the CAMP site for 19 days at the beginning of April 2013. The temperature within the UPOD enclosure over this period varied from 0C to 35C with an average temperature of 14C. The absolute humidity mol fraction in the enclosure varied from 0.003 mol/mol to 0.011 mol/mol with an average of 0.007 mol/mol.

A predicted resistance was calculated using 6.13 with the colocation reference concentration and the lab generated parameters. 6.9 shows the predicted versus measured resistance for one MICS-5525 sensor. Each data point corresponds to a one minute average over the 19 day period. No R_o normalization factor or sensor heater drift compensation was used in the initial prediction.

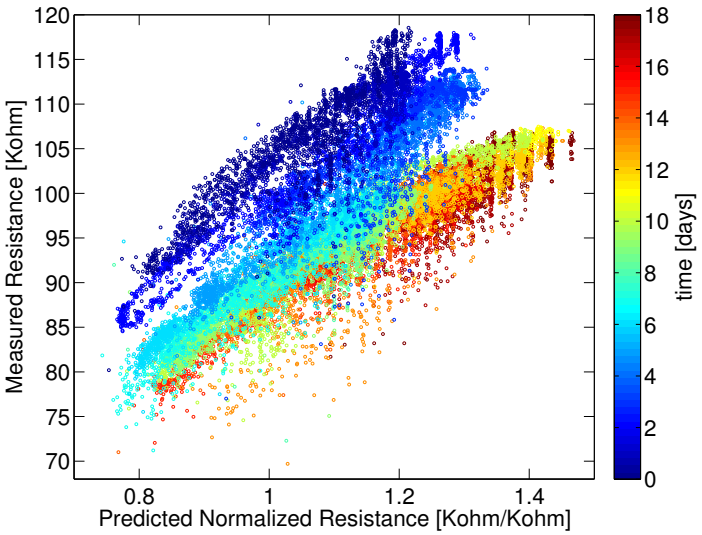

Figure 6.9: MICS-5525 Measured vs. Predicted Resistance with Lab Parameters

The lab parameters do well in linearizing the relationship between the predicted and measured resistance, yet it can be seen that significant temporal drift exists when there is no compensation for the change in heater resistance.

Optimal parameters were generated using the NonLinearModel fitting algorithm in Matlab and minimizing the residual between observed and predicted sensor resistance. The model form 6.13 was again used to predict sensor resistances, except the constant coefficients $\{p_1, ..., p_6\}$ and the

heat transfer coefficient h_t were set as free parameters in a least-square fit of the predicted resistance to the measured resistance. The heater drift correction was also applied to the temperature term as per 6.19. Doing so gives very good agreement between the measured and the predicted resistance as shown in 6.10.

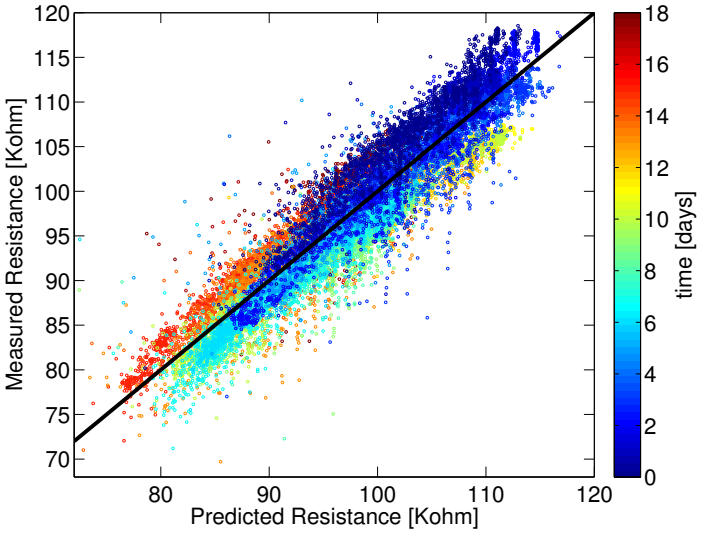

Figure 6.10: MICS-5525 Measured vs. Predicted Resistance with Optimized Parameter

6.1 gives the model parameters from the initial lab experiment and those from the optimization scheme applied to the collocated sensors. Note that p_2 was sufficiently small as to be omitted from the model, and only seven sensor results are presented as one of the collocated sensors broke while in the field.

Table 6.1: Optimized Parameter Values and Prediction Error

Sensor	R_o	p_1	p_3	p_4	p_5	p_6	h_t	RMS
Lab	N/A	-02.07e-02	-4.21e-01	9.90e-01	-1.33e-01	9.00e-04	N/A	N/A
1	101.96	-1.09e-02	-5.26e-01	5.47e-01	-3.01e-01	4.81e-01	9.46e-06	2.98
2	96.02	-1.13e-02	-4.91e-01	4.93e-01	-3.03e-01	5.31e-01	1.13e-05	2.73
3	120.54	-1.39e-02	-6.76e-01	4.88e-01	-4.08e-01	5.46e-01	1.01e-05	3.40
4	121.99	-1.28e-02	-6.51e-01	4.51e-01	-4.26e-01	5.81e-01	9.78e-06	3.37
6	114.44	-1.04e-02	-5.73e-01	6.20e-01	-3.21e-01	4.12e-01	8.18e-06	3.47
7	108.08	-1.02e-02	-5.74e-01	6.13e-01	-3.00e-01	4.15e-01	8.92e-06	3.10
8	117.70	-9.97e-03	-5.75e-01	6.33e-01	-3.16e-01	4.00e-01	7.52e-06	3.36

The value of R_o presented in the table was generated by evaluating the model at 298K with a concentration of zero.

6.0.31 MOx Quantification Model Conclusions

The model form derived in this work does well to predict the sensor response to ambient pollutants while compensating for temperature affects and sensor drift due to changes in the sensor heating element. All sensors of a given type work well with the same model form, yet significant inter-sensor variability requires each sensor to have a unique set of parameter values. Parameter values determined in a lab setting perform poorly when the sensors are deployed in the field. Colocation calibrations are superior in generating optimal model parameter values. The drift of the heating element output must be known in order to compensate for heater drift. This can be achieved by incorporating heater drift in the quantification model, or measuring and adapting the heater output in situ.

Future models should build upon the foundation presented here, incorporating further corrections for humidity, pressure, interference species, etc... Promising approaches include the use of redundant sensors and arrays of sensors with different interference cross-sensitivities.

Bibliography

[1] Joshua Agenbroad. A Simplified Model for Understanding Natural Convection Driven Biomass Cooking Stoves. 2010.

[2] S S Alves and J L Figueiredo. A MODEL FOR PYROLYSIS OF WET WOOD. Chemical Engineering Science, 44(12):2861–2869, 1989.

[3] Hakim Baha and Zohir Dibi. A novel neural network-based technique for smart gas sensors operating in a dynamic environment. Sensors, pages 8944–8960, 2009.

[4] R Bailis. Controlled cooking test (CCT). (August):1–8, 2004.

[5] Rob Bailis, Damon Ogle, N MacCarty, and Dean Still. The Water Boiling Test (WBT). (January):1–38, 2007.

[6] SF Baldwin. Biomass Stoves: Engineering Design, Development, and Dissemination. 1987.

[7] N Barsan and U Weimar. Understanding the fundamental principles of metal oxide based gas sensors; the example of CO sensing with SnO2 sensors in the presence of humidity. Journal of Physics: Condensed Matter, 813, 2003.

[8] Nicolae Barsan and U Weimar. Conduction Model of Metal Oxide Gas Sensors. Journal of Electroceramics, pages 143–167, 2001.

[9] S C Bhattacharya, D O Albina, and Aung Myint Khaing. Effects of selected parameters on performance and emission of biomass- fired cookstoves. Biomass and Energy, 23:387–395, 2002.

[10] N Bruce. Indoor air pollution in developing countries: a major environmental and public health challenge. ...of the World Health ..., 78(9):1078–92, January 2000.

[11] M Bryden, Dean Still, Peter Scott, Geoff Hoffa, Damon Ogle, Rob Bailis, and Ken Goyer. Design principles for wood burning cook stoves. 2005.

[12] H Burnham-Slipper, MJ Clifford, and SJ Pickering. Breeding a Better Stove: the Use of Genetic Algorithms and Computational Fluid Dynamics to Improve Stove Design. ewb-uk.org, 2009.

[13] JP Diebold. A unified, global model for the pyrolysis of cellulose. Biomass and Bioenergy, 34, 1994.

[14] RJ Evans and TA Milne. Molecular Characterization of the Pyrolysis of Biomass. 2. Applications. Energy & fuels, 1(4):311–319, 1987.

[15] Robert J Evans and Thomas A Milne. Moluecular Characterization fo the Pyrolysis of Biomass. 1. Fundamentals. Energy & fuels, 1(2), 1987.

[16] Alfred E. Frey and James S. T'ien. A theory of flame spread over a solid fuel including finite-rate chemical kinetics. Combustion and Flame, 36:263–289, January 1979.

[17] M. Gardon and J. M. Guilemany. A review on fabrication, sensing mechanisms and performance of metal oxide gas sensors. Journal of Materials Science: Materials in Electronics, November 2012.

[18] R Ionescu, A Vancu, and A Tomescu. Time-dependent humidity calibration for drift corrections in electronic noses equipped with SnO 2 gas sensors. Sensors and Actuators B: Chemical, pages 283–286, 2000.

[19] M. Kamionka, P. Breuil, and C. Pijolat. Calibration of a multivariate gas sensing device for atmospheric pollution measurement. Sensors and Actuators B: Chemical, 118(1-2):323–327, October 2006.

[20] Edward J. Kansa, Henry E. Perlee, and Robert F. Chaiken. Mathematical model of wood pyrolysis including internal forced convection. Combustion and Flame, 29:311–324, January 1977.

[21] Hsiang-Cheng Kung. A mathematical model of wood pyrolysis. Combustion and Flame, 18(2):185–195, April 1972.

[22] Craig Lambert. The Way We Eat Now. Harvard Magazine, 2004.

[23] William R. Leonard. Food for Thought. Scientific American, 2012.

[24] JJ Li, Boi Faltings, Olga Saukh, David Hasenfratz, and Jan Beutel. Sensing the Air We Breathethe OpenSense Dataset. pages 2–4, 2012.

[25] Anne E. Lipska and Frank A. Wodley. Isothermal pyrolysis of cellulose: Kinetics and gas chromatographic mass spectrometric analysis of the degradation products. Journal of Applied Polymer Science, 13(5):851–865, 1969.

[26] X Liu, Sitian Cheng, Hong Liu, Sha Hu, Daqiang Zhang, and Huansheng Ning. A survey on gas sensing technology. Sensors, pages 9635–9665, 2012.

[27] C. L'Orange, M. DeFoort, and B. Willson. Influence of testing parameters on biomass stove performance and development of an improved testing protocol. Energy for Sustainable Development, 16(1):3–12, March 2012.

[28] Nicholas Masson. Mobile sensing technology. 2013.

[29] Daniel David Miller-Lionberg. A Fine Resolution CFD Simulation Approach for Biomass Cook Stove Development. 2011.

[30] William J Parker and Susan L Levan. DOUGLAS-FIR AND THE HEAT OF COMBUSTION OF THEIR VOLATILE PYROLYSIS PRODUCTS and. Wood and Fiber Science, 21(3):289–305, 1989.

[31] Eva Rehfuess, Sumi Mehta, and Annette Prüss-Üstün. Assessing Household Solid Fuel Use: Multiple Implications for the Millennium Development Goals. Environmental Health Perspectives, 114(3):373–378, January 2006.

[32] AF Roberts. A review of kinetics data for the pyrolysis of wood and related substances. Combustion and Flame, 272, 1970.

[33] et al. T.B. Reed. Survey of Biomass Gasification. Solar Energy Research Institute/DOE, 1979.

[34] Henrik Thunman, F Niklasson, F Johnsson, and B Leckner. Composition of Volatile Gases and Thermochemical Properties of Wood for Modeling of Fixed and Fluidized Beds. Energy & fuels, pages 1488–1497, 2001.

[35] F Thurner and U Mann. Kinetic investigation of wood pyrolysis. Industrial & Engineering Chemistry Process ..., pages 482–488, 1981.

[36] VITA. Testing The Efficiency Of Wood-Burning Cookstoves: Provisional International Standards. 1985.